Modeling the response to external stimuli of the zebrafish's optic tectum neurons with avalanche-like spontaneous activity

Mateo Amortegui
Université Paris-Saclay
mateo.amortegui-cifuentes@universite-paris-saclay.fr

Supervisors:
Germán Sumbre
Institut de biologie de l'Ecole normale supérieure (IBENS)
sumbre@bio.ens.psl.eu
Adrián Ponce-Alvarez
Polytechnic University of Catalonia, Department of Mathematics
adrian.ponce@upc.edu

June 16, 2024

Abstract

Previous studies found that the zebrafish spontaneous whole-brain neuronal dynamics, obtained with Ca2+ imaging, is avalanche-like, i.e., it has alternating periods of silence and collective cascading activity bursts, where both the duration of the bursts and the number of neurons that spiked during those bursts follow power law distributions with exponents close to the random field Ising universality class, but which deviate from their critical values for avalanches occurring when there is an unbalance between excitatory (E) and inhibitory (I) activity. Here, we model the response of the zebrafish neurons in the optic tectum, displaying avalanche dynamics in spontaneous activity, to an external stimulus, aiming to see whether the power law exponents change or if the dynamics is no longer avalanche-like, and how this is related to E/I unbalances. For this, we simulated the avalanche dynamics of a network of excitatory and inhibitory stochastic neurons with the stochastic Wilson-Cowan model, taking the connectivity matrix as function of data of the position of neurons in the optic tectum, and we found values of the parameters of the model that reproduce the experimental power law exponents. Then, we varied the value of the parameter representing the external input to neurons, e.g., an optogenetic stimulus, for various proportions of stimulated E or I neurons. We found that as the stimulus to the E neurons grows, the inhibition maintains the E/I balance and that avalanches get longer, until reaching a Poissonian regime. On the other hand, an increasing stimulus to the I neurons shortens avalanches and the E/I ratio, until E neurons get totally inhibited. Surprisingly, for reasonably high but balanced stimulus to E and I neurons, avalanche dynamics remains unchanged.

1 Introduction

1.1 What are neural avalanches and why are they important

A neuronal avalanche is commonly defined as a period of continuous collective cascading bursts of activity of a network of neurons, preceded and followed by a total absence of activity (Beggs and Plenz [2003]). The study of these avalanches can be tried to be seen as analogous to the study of out-of-equilibrium second order phase transitions in physics (e.g. in ferromagnets), as one aims to understand neuronal activity that seems to be close to a critical point between a low order or low "firing synchrony" phase and a high order phase. One may roughly characterize the low order phase by a firing pattern of the network of neurons similar to a collection of independent Poisson processes, analogous to the $T > T_c, m(t) = 0$ phase in ferromagnets and the ordered phase by "trivially" synchronized sustained firing of highly correlated neurons analogous to $T < T_c, m(t) \pm 1$. However, one shall always have in mind that neurons are far from being idealized Ising spins, e.g., they do not have the same ± 1 symmetry as they remain in a quiescent state integrating inputs from other neurons, only firing when the input exceeds a threshold, and the interactions between neurons are not symmetric either. Pushing the analogy, close enough to the critical point, the dynamics of the network is that of neuronal avalanches, i.e., periods of cascading firing that can extend up to the system size which are preceded and followed by periods of no or very low firing, while the correlations between the neurons' spike time series during the whole experiment remain low with respect to the high order phase. The distributions of the number of spikes during the avalanches, called the avalanche size, and of the duration of the avalanches seem to follow scale-invariant power-law distributions with cut-offs that scale with the system size, suggestive of criticality.

There is a growing corpus of experimental observations of neuronal avalanches, from the local field potentials recordings of spontaneous neuronal activity in cultures of slices of rat cortex (Beggs and Plenz [2003]), high resolution electrophysiology data of cultures of slices of cortical tissue from living rats (Friedman et al. [2012]), local field potentials of the superficial layers of the cat's cortex during spontaneous activity under anesthesia (Hahn et al. [2010]), spontaneous cortical activity in awake monkeys (Petermann et al. [2009]), up to the zebrafish larvae whole-brain spontaneous activity (Ponce-Alvarez et al. [2018]). Another compelling point is that the brain could benefit of operating near to a critical state, e.g, by having bigger repertoires of neural activity patterns, bigger mutual information between external stimuli and neural activity, and responding to a bigger range of stimuli (reviewed in Shew and Plenz [2013]). However, there is still no consensus on whether neurons operate near a bona fide critical point, e.g., the methodologies for assessing the criticality of a system have been questioned (Destexhe and Touboul [2021]), and major questions of research are still to better determine relevant order and control parameters, or, in the case self-organized criticality hypotheses, biological mechanisms (e.g., plasticity) that would tune the system towards the critical point.

Ongoing work (Ponce-Alvarez et al., unpublished) analyzed one-hour 15Hz recordings of the spontaneous activity of $N \sim 2000$ neurons in the zebrafish optic tectum, for ten fish larvae, obtained with calcium fluorescence selective-plane illumination microscopy. They binarized the fluorescence fluctuations signal $\Delta F/F$ by setting it to 1 when the signal is 3 standard deviations above from baseline fluctuations, and 0 otherwise. The resulting binarized calcium fluorescence events show avalanche dynamics (Fig. 1). Using both spatially constrained and unconstrained definitions of neural avalanches with activity

thresholds (see Definitions in 2.4), they found that the distributions of avalanche size S and duration T, and the relation between the average S given T, are will fit by power laws $P(S) \sim S^{-\tau}, P(T) \sim T^{-\alpha}, < S > (T) \sim T^{\frac{1}{\sigma\nu z}}$ which span several decades, suggestive of criticality. For the spatially constrained definition, the power law exponents are close to those of the universality class of the non-equilibrium random field Ising model, whereas for the spatially unconstrained definition, the exponents, averaged over the ten fish data, are $< \alpha >= 1.64 \pm 0.02, < \tau >= 1.62 \pm 0.04, < \sigma\nu z >= 0.87 \pm 0.03$ (Fig. 2), which agree with previous results (Fontenele et al. [2019], Fosque et al. [2021]). Additionally, we have seen that, under the spatially unconstrained definition, the distribution of the duration of silences D (i.e., total absence of activity of the network) seems to be a power law $P(D) \sim D^{-\gamma}$ with $< \gamma >= 1.99$. Notably, they looked at the E/I ratio, defined as the proportion of active excitatory neurons divided by the proportion of active excitatory and inhibitory neurons at a given time, which is a candidate control parameter for avalanche dynamics (Plenz et al. [2021]), and found that the power law exponents deviate from their critical values for avalanches occurring at unbalanced E/I ratios (Fig. 3).

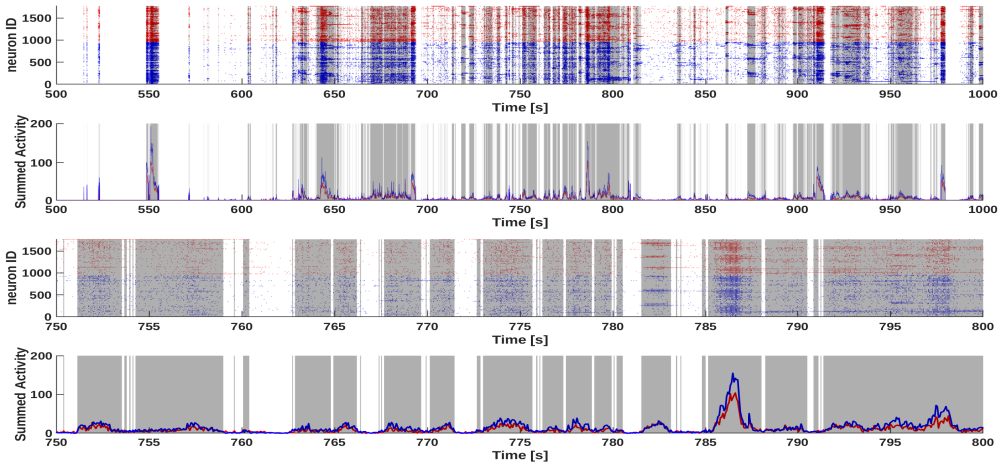

Figure 1: Sample rasters of the binarized calcium fluorescence events and their corresponding summed activity of excitatory (blue) and inhibitory (red) populations, shown for two time scales of 500s and 50s. The shaded patches correspond to the time intervals of the avalanches, during which the sum of the excitatory together with the inhibitory activity was superior to a threshold of 0.5% of the total number of neurons

Here, we aim to investigate how external stimuli could perturb the spontaneous activity of the zebrafish's optic tectum neurons, e.g., displacing it out of its avalanche dynamics, and to see how this could be related to perturbations in the E/I balance. For this, we modeled the resting state spiking activity of the neurons with a network of excitatory (E) and inhibitory (I) neurons following the stochastic Wilson-Cowan model (Benayoun et al. [2010], 2.1), using the positions of the neurons to generate the connectivity matrix, and then converted the spikes to binarized calcium fluorescence events (2.3). Once we found parameters that generated activity with power law statistics similar to the experimental statistics, we explored how the avalanche dynamics and E/I balanced changed when varying the parameter of external input to different proportion of E and I neurons, and found similar changes as those found in the spontaneous activity experimental data.

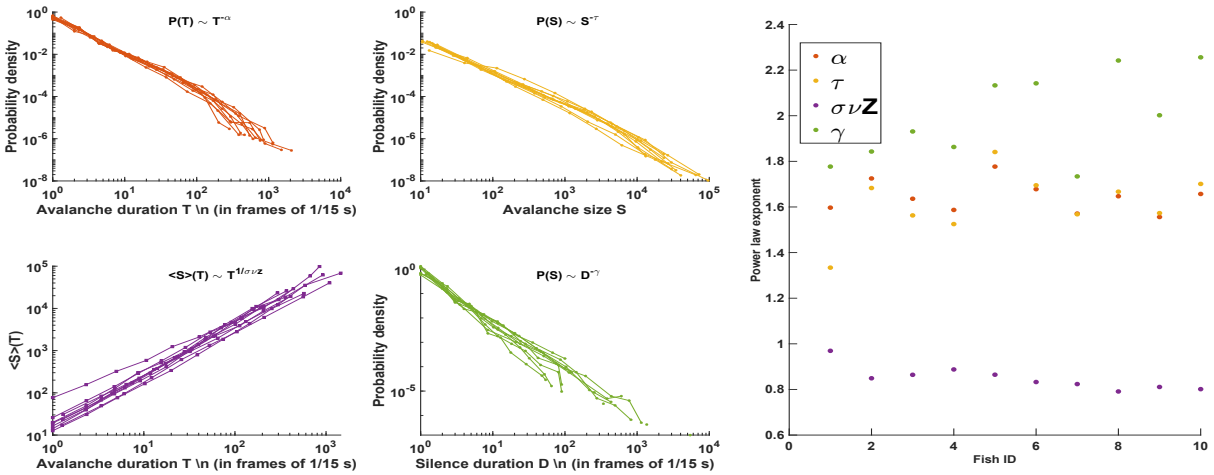

Figure 2: Data for ten fish of the distributions of avalanche size, duration, silence duration D, and relation between average avalanche size given the avalanche size, showing power law statistics. Here, the spatially unconstrained definition is used (see 2.4)

2 Methods

2.1 Model of the avalanche dynamics of the zebrafish's neurons

We modeled the avalanche dynamics of the zebrafish's optic tectum neurons with the stochastic Wilson-Cowan model (Benayoun et al. [2010]). This model considers a network of N_E excitatory (E) neurons and N_I inhibitory (I) neurons, where each neuron $i = 1...N \equiv N_E + N_I$ can be in an active ($a_i(t) = 1$) or a quiescent ($a_i(t) = 0$) state. There is a pairwise coupling between the neurons represented by a connectivity matrix W, where $w_{ij,i\neq j}$ is the synaptic weight between the presynaptic neuron j and the postsynaptic neuron i, where $w_{ij} \geq 0$ if the presynaptic neuron is excitatory, $w_{ij} \leq 0$ if the presynaptic neuron is inhibitory, and $w_{ii} = 0$. Each neuron i receives an input $s_i(t) \equiv \sum_{j=1}^{N} w_{ij}a_j(t) + h_i(t)$ from other neurons and from the exterior field. The state of the neurons evolves in time as continuous-time Markov process with two possible transitions determined by their probability transition rates : one transition is the so-called spike $a_i = 0 \overset{gf(s_i(t))}{\rightarrow} a_i = 1$, where g is a constant and homogeneous probability rate and

$$f(x) = \begin{cases} \tanh(x) & \text{if } x > 0, \\ 0 & \text{if } x < 0. \end{cases}$$

is the response function, and the other transition is called a decay $a_i = 0 \underset{q}{\leftarrow} a_i = 1$ where q is the constant and homogeneous decay probability rate. This means that for a time $\Delta t \to 0$, $\mathbb{P}(a_i(t) = 1 \to a_i(t + \Delta t) = 0) = q\Delta t$ and $\mathbb{P}_i(a_i(t) = 0 \to a_i(t + \Delta t) = 1) = gf(s_i(t))\Delta t$.

In Benayoun et al. [2010], they consider the case of all-to-all connectivity, with $N_E = N_I = N$, $h_i(t) = h > 0$, $g = 1ms^{-1}$, $w_{ij,j\in E} \equiv \frac{w_E}{N}$, $w_{ij,j\in I} \equiv \frac{-w_I}{N}$, i.e., $s_i(t) = w_E\frac{\sum_{j\in E} a_j(t)}{N} - w_I\frac{\sum_{j\in I} a_j(t)}{N} + h \equiv w_E E - w_I I + h$, where here there is a different use of notation for E, I, which now represent the proportion of active excitatory and inhibitory neurons. By doing a gaussian approximation, they express the total amounts k and l of excitatory and inhibitory neurons as an extensive deterministic term plus some subextensive noise, $k = NE + \sqrt{N}\xi_E$, $l = NI + \sqrt{N}\xi_I$. where the deterministic term follows the Wilson-Cowan equations (Wilson and Cowan [1972]), which do not themselves

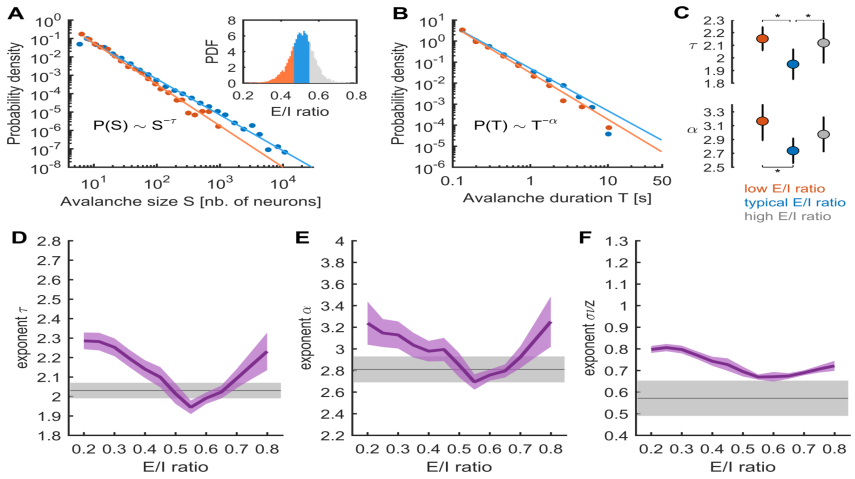

Figure 3: Figure and caption from unpublished work, using a spatially-constraint definition of avalanches, from Ponce-Alvarez et al. **Neuronal avalanche exponents as a function of the E/I ratio. A)** Distribution of avalanche sizes (S) for avalanches occurring at low E/I ratios (red, lowest 25% E/I ratios) and at typical E/I ratios (blue, E/I ratios within the 25th-75th percentiles). Solid lines indicate estimated power laws. Inset: distribution of E/I ratio. Red: low E/I ratios; blue: typical E/I ratios; gray: high E/I ratios (highest 25% E/I ratios). **B)** Distribution of avalanche durations (T) for avalanches occurring at low and typical E/I ratios, respectively. Solid lines indicate estimated power laws. **C)** Power-law exponents describing the distributions of the sizes (τ, top panel) and durations (α, bottom panel) of neuronal avalanches occurring at low, typical, and high E/I ratios. One-way ANOVA: for exponent τ: $F(2,27) = 7.35$, $p = 0.003$; for exponent α: $F(2,27) = 7.94$, $p = 0.002$. *: $p < 0.05$, post hoc t tests. **D-F)** Average power-law exponents τ, α, and $\sigma\nu z$ estimated for different bins of E/I ratios. For each fish, the E/I ratio bins were chosen to contain an equal number of neuronal avalanches (1,000). The center of the bins was defined as the mean E/I ratio associated to the corresponding neuronal avalanches. The relation between exponents and E/I ratio was linearly interpolate before averaging over fishes. Purple shaded areas indicate SEM. The gray horizontal lines and shaded areas indicate the expected critical exponents and their uncertainty, respectively, in random field Ising models

produce avalanches. After the change of variables $\Sigma = \frac{E+I}{2}, \Delta = \frac{E-I}{2}$, they show the deterministic fixed point is $(\Sigma_0 \neq 0, \Delta_0 = 0)$ and after a linear noise approximation, they show that the fluctuations ξ_Σ, ξ_Δ around that fixed point follow :

$$\begin{pmatrix} \xi_\Sigma \\ \xi_\Delta \end{pmatrix} = \begin{pmatrix} -\lambda_1 & w_{ff} \\ 0 & -\lambda_2 \end{pmatrix} \begin{pmatrix} \xi_\Sigma \\ \xi_\Delta \end{pmatrix} + \sqrt{q\Sigma_0} \begin{pmatrix} \eta_\Sigma \\ \eta_\Delta \end{pmatrix}$$

where $w_{ff} = (1 - \Sigma_0)(w_E + w_I)f'(s_0)$, with $s_0 = (w_E - w_I)\Sigma_0 + (w_E + w_I)\Delta_0 + h = (w_E - w_I)\Sigma_0 + h$ the input at the fixed point, $\lambda_1 = (1 - \Sigma_0)(w_E - w_I)f'(s_0) + q + f(s_0)$, $\lambda_2 = q + f(s_0)$, and where the matrix comes from the Jacobian of the deterministic equations evaluated at the fixed point. This means that the fixed point $(\Sigma_0, 0)$ is less stable as w_- is smaller, and that deviations from the balance between excitation and inhibition, represented by ξ_Δ, drive the fluctuations of the mean variable ξ_Σ, and that this feedforward effect is greater as $w_{ff} \propto w_+$ is bigger, which explains why avalanches occur when $w_+ \equiv w_E + w_I \gg w_- \equiv w_E - w_I$ (Fig. 4 A,B,C), but only for N not too big (e.g. $N < 10^5$) so that the deterministic, non-avalanche-like part, does not dominate the fluctuations. In summary, we can see the dynamics of the system as the fluctuations around a fixed point ($E_0 = I_0 \neq 0$) which gets closer to a line attractor (i.e., its nullclines increasingly overlap) as w_+ increases (Fig. 4 G,H,I) and whose stability decreases as w_- decreases, where one has not assumed some self-organized criticality mechanism, but where one has assumed a hidden feedforward connectivity from the fluctuations in the difference variable to the fluctuations in the sum variable.

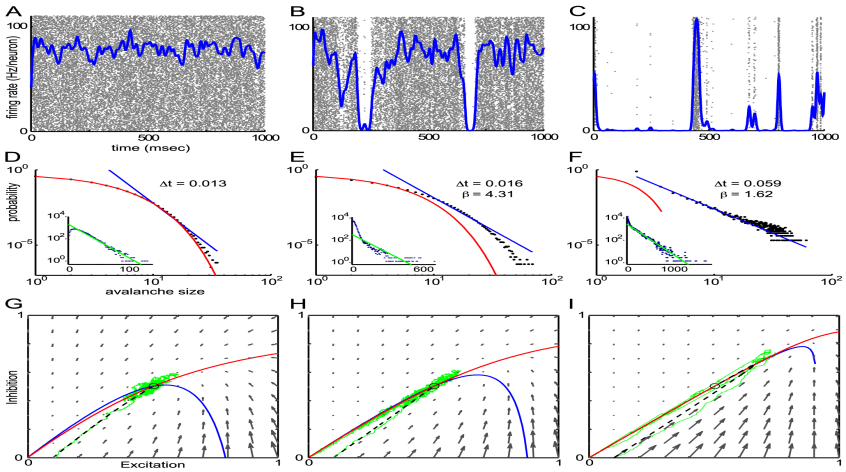

Figure 4: Figure and caption from Benayoun et al. [2010] : Transition from asynchronous firing to avalanche dynamics. Simulations with parameter values $h_E = h_I = 0.001$, $w_E - w_I = 0.2$, and $N = 800$. Left column, $w_E + w_I = 0.8$, middle column, $w_E + w_I = 1.8$, right column $w_E + w_I = 13.8$. A,B,C: Mean firing rate of network plotted over raster plot of spikes. Individual neurons correspond to rows, and are unsorted except that the lower rows represent excitatory neurons and the upper rows inhibitory. D,E,F: Network burst distribution in number of spikes, together with geometric (red) and power law (blue) fit; Δt , the mean inter spike interval, is the time bin used to calculate the distribution, and β is the exponent of the power law fit. Inset, inter-spike interval (ISI) distribution in ms for a sample of 50 neurons from the network, shown in semi-logarithmic co-ordinates, with exponential fit (green). G,H,I: Phase plane plots of excitatory and inhibitory activity showing the vector field (grey) and nullclines $\dot{E} = 0$ (red) and $\dot{I} = 0$ (blue), of the associated Wilson-Cowan equations and plots of a deterministic (black dashed) and a stochastic (green) trajectory starting with identical initial conditions. Note that the deterministic fixed point (black circle), where the nullclines cross, does not change as $w_E + w_I$ increases, but the angle between the nullclines becomes increasingly shallow, and the stochastic trajectory becomes increasingly spread out.

2.1.1 Connectivity matrix as a function of experimental data

We generate the connectivity matrix W as a function the distance between the neurons and of their type, E or I, known from the experimental data. Note that this a main difference with the previous theory work of Benayoun et al. [2010] and de Candia et al. [2021b], where they analyze an all-to-all connectivity matrix.

We first build an adjacency matrix C by supposing that the probability of neuron j to be a presynaptic neuron of neuron i decays exponentially with the distance :

$$c_{ij} = \begin{cases} 1 & \text{if } e^{-\frac{d(\underline{r}_i, \underline{r}_j)}{\lambda}} > l, l \sim \mathrm{U}[0,1], \\ 0 & \text{otherwise .} \end{cases}$$

where $\underline{r}_i$ is the 3D position vector of the neuron i, d is the cartesian distance function, and λ is the parameter of typical length of decay of the connection. Note that it is then not necessarily a symmetric matrix because the random number l is drawn two separate times for each pair (i,j).

The connectivity matrix W is a rescaling of the adjacency matrix :

$$w_{ij} = \begin{cases} \frac{w_E}{N_{E,pre}(i)} & \text{if } c_{ij,j\in E} = 1 \\ \frac{-w_I}{N_{I,pre}(i)} & \text{if } c_{ij,j\in I} = 1 \\ 0 & \text{if } c_{ij} = 0 \text{ or } i = j. \end{cases}$$

with $N_{E,pre}(i) = \sum_{j\in E, j\neq i} c_{ij}$, i.e., the number of presynaptic E neurons of neuron i and $N_{I,pre}(i) = \sum_{j\in I, j\neq i} c_{ij}$ the number of presynaptic I neurons of neuron i, where $w_E > 0$ and $w_I > 0$ are parameters of the model. In this way, for any postsynaptic neuron i, the sum of the weights of all its presynaptic E neurons is w_E, i.e., $\sum_{j\in E} w_{ij} = w_E \geq 0$ and similarly, $\sum_{j\in I} w_{ij} = -w_I \leq 0$, and $w_{ij,j\in E} \gtrsim \frac{w_E}{N_E}$, $-w_{ij,j\in I} \lesssim \frac{-w_I}{N_i}$ (with equalities in the all-to-all connectivity limit $\lambda \to \infty$). So, at any time, $-w_I + h_i(t) \leq s_i(t) \leq w_E + h_i(t)$ with equality on the right when all presynaptic E neurons are active and all presynaptic I neurons are quiescent, and with equality on the left when all presynaptic I neurons are active and all presynaptic E neurons are quiescent, and $s_i(t) = w_E - w_I + h_i(t)$ if all presynaptic neurons are active.

For some fixed values of the model's parameters, the power law exponents of the simulated avalanche dynamics vary greatly when using different adjacency matrices generated as a function of the different data of the position of the neurons of different fishes, and even some simulations do not produce avalanche dynamics for those fixed values of the parameters (5.1). Thus, to simplify the analysis when varying parameters, we only used the data of the positions of the neurons of one particular fish to generate connectivity matrices (Fig. 5a). For the position of the neurons of that fish and for the values of the parameter $\lambda \sim 80\mu$m that we commonly used in simulations, the connectivity matrix is relatively sparse (Fig. 5), where each neuron has roughly $\frac{N_{E,pre}(i)}{N_E} \approx \frac{N_{I,pre}(i)}{N_I} \approx \frac{1}{4}$ (Fig. 5c).

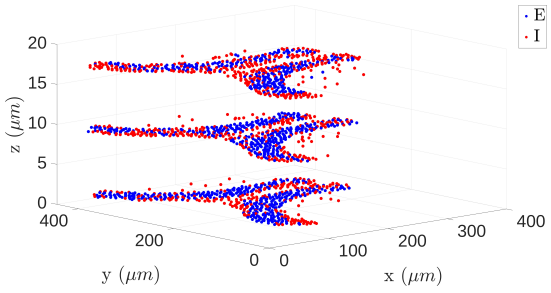

(a) Positions of the neurons.

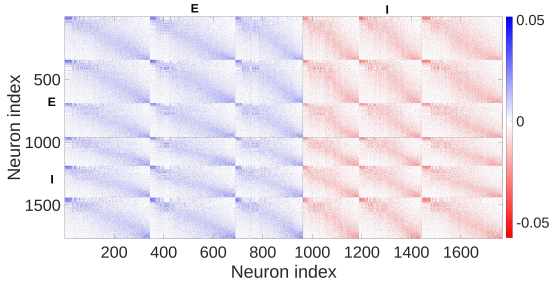

(b) Connectivity matrix. Its 3x3 grid substructures arise because both the E and I neurons are labeled by order in the z coordinate.

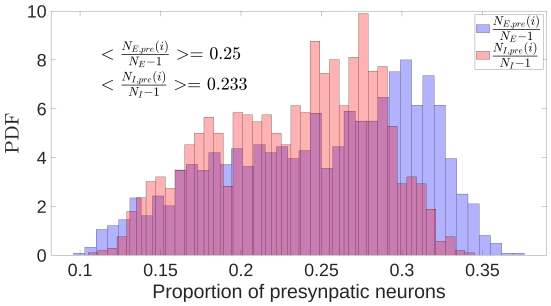

(c) Distributions of the proportions of E and I presynaptic neurons $\frac{N_{E,pre}(i)}{N_E-1}$ and $\frac{N_{I,pre}(i)}{N_I-1}$

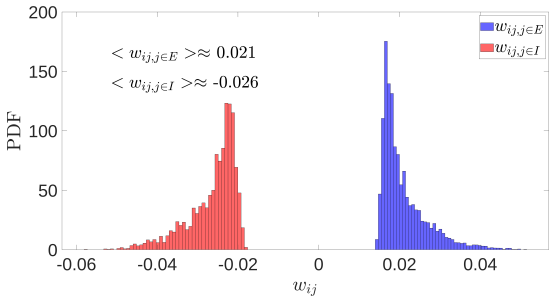

(d) Distributions of the non-zero weights.

Figure 5: One example of generating a connectivity matrix as a function of the position of the neurons for $\lambda = 80\mu m$, $w_E = 5.045$, $w_I = 4.955$, $N_E = 962$, $N_I = 806$.

The value of $\lambda \sim 80\mu$m used in simulations, which was chosen to match the experimental values of the power law exponents (see 3.1), was also corroborated by comparing the Pearson correlation between the time series of the neurons of the spontaneous activity $\Delta F/F$ data as a function of the distance between neurons with the null model of shuffled

correlation values. We found that the average lines cross at around $\lambda \sim 90\mu$m for all 10 fish (e.g. Fig. 6).

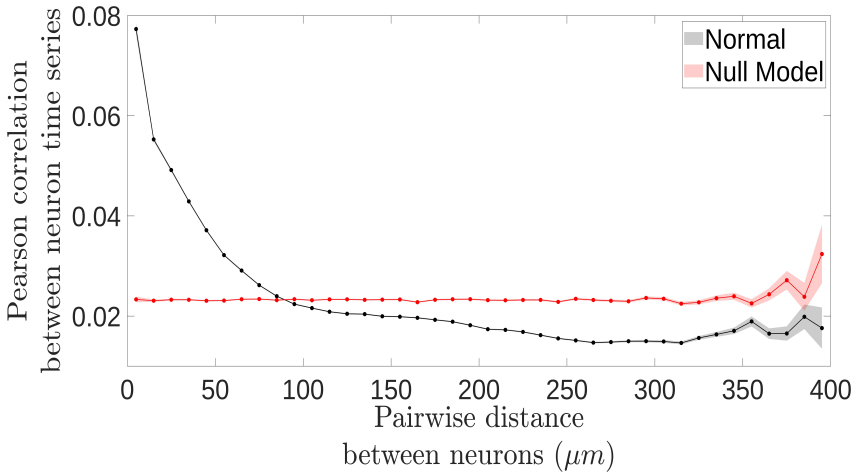

Figure 6: Example for one fish of the Pearson correlation coefficient between the time series of the neurons of the spontaneous activity $\Delta F/F$ data as a function of the pairwise distance between neurons. The solid line represents the mean values over bins of 10μm. The shaded area represents the standard error of the mean over the same bins. The null model in red is done by shuffling the vector of correlation values. The cross between the normal and the null model mean lines is at $\sim 90\mu$m

2.2 Simulation algorithm of the stochastic Wilson-Cowan model

We simulate the stochastic Wilson-Cowan model using the Gillespie algorithm (Gillespie [1977]) (Algorithm 1). One assumes that the evolution of each neuron i follows a Poisson distribution of rate $r_i(t)$:

$$r_i(t) = \begin{cases} q & \text{if } a_i(t) = 1, \\ gf(s_i(t)) & \text{if } a_i(t) = 0. \end{cases}$$

Algorithm 1 Gillespie algorithm

1: Set $t = 0$
2: Set the initial states of the neurons $\{a_i(t = 0)\}$.
3: Calculate the initial rates of the neurons $\{r_i(t = 0)\}$.
4: **while** $t < t_{final}$ **do**
5: Draw $\Delta t \sim \text{Exp}(\sum_{i=1}^{N} r_i(t))$
6: Pick a unique neuron to change its state, where any neuron i has a probability $\frac{r_i(t)}{\sum_{i=1}^{N} r_i(t)}$ to be selected.
7: Do $t = t + \Delta t$
8: Update the rates $\{r_i(t)\}$ of the neurons.
9: **end while**

In this way, one generates a set of times and neuron indices of each transition, out of which we only retain the indices and times of the spiking transitions $a_i(t) = 0 \to a_i(t) = 1$ as these are the only events relevant for analyzing the avalanches. We choose the initial states of the neurons to be 30% active at random. Note that in this algorithm, time is a continuous variable. Time delays are not considered, as the inputs to the postsynaptic

neurons change at exactly the same time the state of the presynaptic neuron changes. We tried to get rid of the effect of initial conditions by ignoring the transient activity of the simulated network for any data analysis, including power-law fittings, for $t \in [0, t_{eq}]$, where t_{eq} is a parameter commonly set to $t_{eq} \sim 100$ s. The experimental recordings lasted 3600 s, however, the power law exponents of a shortened version of the data for $t \in [0, 2000]$ s, averaged over the ten fish, only change of ± 0.03 with respect to the exponents of the full data, which is much less than the variations of $\sim \pm 0.1$ due to the simulation stochasticity, thus, simulations were done with $t_{final} = 2000$ s to save time.

2.3 Transformation of spiking events to Calcium fluorescence binary events

After having generated the spiking binary events of the network with the Gillespie algorithm, we transform them to a $\Delta F/F$ Calcium fluorescence signal using the phenomenological Spike-to-fluorescence model of Wei et al. [2020]. In that model, for a given neuron, one calculates a latent variable $c(t)$ by convolving its spiking times $\{t_1 ... t_k\}$ with a double exponential kernel and adding a gaussian noise $\eta_1(t) \sim \mathcal{N}(0, \sigma_1^2)$, i.e. $c(t) = \sum_{t>t_k} (1 - e^{-(\frac{t-t_k}{\tau_r})}) e^{-(\frac{t-t_k}{\tau_d})} + \eta_1(t)$, where τ_r and τ_d are the rise and decay time parameters of the double exponential. We calculate $c(t)$ using a time bin of 0.01 seconds. We choose σ_1 to be 10% of the mean "latent activity" of the whole network, i.e., if we call $c_i(t_j)$ the value of the latent variable of neuron i (before adding the noise) at time bin j, then $\sigma_1 = \frac{1}{10} \sum_{i=1}^{N} \sum_{j=1}^{J} \frac{c_i(t_j)}{N \cdot J}$ where J is the total number of time bins. Given that the Calcium indicator used in the experimental data we considered was the H2B-GCamP6f, according to Shemesh et al. [2020], we use $\tau_r = 0.5$ s and according to Kawashima et al. [2016] and Duchemin et al. [2021], we use $\tau_d = 3$ s.

Then, the $\Delta F/F(t)$ is a sigmoid of the latent variable plus some gaussian noise $\eta_2(t) \sim \mathcal{N}(0, \sigma_2^2)$, i.e., for a neuron i, $(\Delta F/F(t))_i = \frac{F_{max}}{1+e^{k \cdot (c_i(t) - c_{1/2})}} + \eta_2(t)$, where F_{max}, k and $c_{1/2}$ are the maximum-value, slope and half-activation parameters of the sigmoid. We use $F_{max} = 10$, $k = 0.6$ and $c_{1/2} = 5$. Once again, we choose η_2 as 10% of the mean fluorescence activity of the whole network, i.e. $\sigma_2 = \frac{1}{10} \sum_{i=1}^{N} \sum_{j=1}^{J} \frac{(\Delta F/F(t))_i(t_j)}{N \cdot J}$. Then, in order to have a signal of the same temporal resolution of the data, we coarse-grain the $\Delta F/F(t)$ signal by taking its average over time bins of length $\frac{1}{15}$ s.

Finally, to transform the fluorescence continuous signal to fluorescence binary events ("Calcium spikes"), for each neuron i, we use as a threshold the z-score $z_i(t)$ of its $(\Delta F/F)_i(t)$ signal (as in Romano et al. [2017]), i.e. $z_i(t) = \frac{(\Delta F/F)_i(t) - <(\Delta F/F)_i(t)>_{time}}{\sqrt{<((\Delta F/F)_i(t) - <(\Delta F/F)_i(t)>_{time})^2>_{time}}}$:

$$(\Delta F/F)_i(t) = \begin{cases} 1 & \text{if } z_i(t) \geq 3, \\ 0 & \text{if } z_i(t) < 3. \end{cases}$$

2.4 Definition of neural avalanches

Commonly, a neuronal avalanche is defined as a period of continuous activity of the network preceded and followed by a total absence of activity, where one does not take into account the position of the neurons (e.g. Beggs and Plenz [2003]). The time elapsed during the period of activity is called the avalanche duration, and the number of spikes that occurred during the avalanche is called the avalanche size. As we analyze data from three very close planes ($\delta z \approx 10 \mu m$) of the region of the optic tectum $\delta x \approx \delta y \approx 400 \mu m$,

we use this spatially unconstrained definition of avalanches rather than a definition where one would impose a maximal distance to consider that two active neurons form part of a common avalanche. However, because in the optic tectum, even in the resting state, there are stimuli coming from other zones of the brain, we impose that there is always some external input to the network, i.e., for any neuron i, there are times at which $h_i(t) \neq 0$, and so a dead network $\{a_i(t) = 0$ for all $i = 1...N\}$ is not an absorbing state. This motivates adding a threshold to the spatially unconstrained definition of avalanches (e.g. as in Poil et al. [2012]) to filter out noisy activation of the network caused by the external inputs, in an attempt to label only the "truly" cascading synchronous events as avalanches. In this definition, an avalanche is occurring at a given time bin if the sum of the active neurons is above a threshold (Algorithm 2):

Algorithm 2 Getting the sizes and durations of avalanches according to the non-spatial threshold definition of avalanche

Inputs:
  t : time array of L elements $[t_1, ...t_L]$
  SummedActivity: array of L elements whose i-th element contains the number of neurons active at time bin i, i.e., SummedActivity(i) $= \sum_{k=1}^{N} a_k(t_i)$, $i = 1...L$
  th: avalanche threshold (in number of neurons)
Outputs:
  Size: array containing the sizes of the avalanches
  Duration: array containing the durations of the avalanches
Initialization:
Size $\leftarrow$ [ ]
Duration $\leftarrow$ [ ]
$s \leftarrow 0$
$d \leftarrow 0$
for $i = 2$ to L **do**
  if $SummedActivity(i) \geq th$ **then**
    $s \leftarrow s + SummedActivity(i)$
    $d \leftarrow d + 1$
  else if $SummedActivity(i) < th$ **and** $SummedActivity(i-1) \geq th$ **then**
    Size $\leftarrow$ append(Size, s)
    Duration $\leftarrow$ append(Duration, d)
    $s \leftarrow 0$
    $d \leftarrow 0$
  end if
end for
Size $\leftarrow$ Size[Duration > 0]
Duration $\leftarrow$ Duration[Duration > 0]
Return [Size, Duration]

We use the resolution of the fluorescence binary events, $\frac{1}{15}$ s, for the time bin size for the fluorescence avalanches, and a much bigger time bin size of 0.5 s when analyzing spike avalanches (the maximum bin size up to which critical exponents are robust as discussed in Fontenele et al. [2024]) and in both cases $\lfloor \frac{5}{1000} \cdot N \rfloor$ for the avalanche threshold.

2.5 Power-law fitting

For estimating the power law exponents of the avalanche size and duration probability distributions, they were fitted by truncated power laws $P(S) \sim S^{-\tau}$ and $P(T) \sim T^{-\alpha}$ using the maximum likelihood estimation (MLE) function from the MATLAB NCC (Neural Complexity and Criticality) Toolbox (Marshall et al. [2016]) with [min(S),max(S)] and [min(T),max(T)] as left and right cutoffs. The function $< S(T) > \sim T^{\frac{1}{\sigma}}$ was calculated by averaging S and T over logarithmically spaced bins in the range [min(T),1.1 max(T)], and its power law exponent was obtained by linear least squares of log(S) vs log(T). Depending on the parameters of the model, avalanche distributions of the simulated networks did not always seem to follow clear power laws, and because in this work we do not take into account the uncertainty of the power laws, we required a minimum of either 5 avalanches or both 3 avalanches and a range of durations greater than one decade to consider valid the power law exponent, otherwise it was set to NaN. This criterion was found to be satisfactory by qualitative inspection of the distributions. Additionally, we found that when there are no spike avalanches, the noise introduced by the algorithm when transforming spikes to calcium fluorescence binary events can constitute avalanches by itself, and so when the τ,α,$\sigma\nu z$ exponents for spike avalanches are NaN, they are also set to NaN for calcium events.

2.6 Averages over simulations

When doing k batches of simulations B^k of the SWC, where in each batch B^i we vary n parameters P_j of the model but without varying λ, (i.e., in B^i_λ we vary $P_1, ..., P_n, P_j \neq \lambda$), we generate a unique adjacency matrix C^i_λ for all simulations of B^i_λ (which may be then normalized in different ways if varying the parameters w_E or w_I). So, when we say that a result with parameters $(P_1 = p_1, ..., P_n = p_n)$ was obtained after taking the average over k simulations, it refers to averaging over the "randomness of the k connectivity matrices" of the k batches of simulations, i.e. the average of the results obtained with $((P_1 = p_1, ..., P_n = p_n), C^1_\lambda)$, ..., $((P_1 = p_1, ..., P_n = p_n), C^k_\lambda)$.

3 Results

3.1 Simulations of the spiking and fluorescence neuronal spontaneous activity that reproduce the experimental avalanche statistics

We found value ranges of the parameters (e.g. $w_+ = 10$, $w_- = 0.09$, $g = 1Hz$, $q = 0.1Hz$, $h = 0.001, \lambda = 80\mu m$) of the stochastic Wilson-Cowan model that generate avalanches of spikes, which after transformation to binarized calcium fluorescence events (see 2.3), produce avalanches (Figs. 8, 9, 10) with power-law distributions spanning over several decades with exponents close to the experimental exponents and with similar standard deviation of the normalized summed excitatory and inhibitory activity (Fig. 7). The values used as a reference for the experimental exponents are the values of the particular fish used for generating the connectivity matrix, and not the average ones in the introduction.

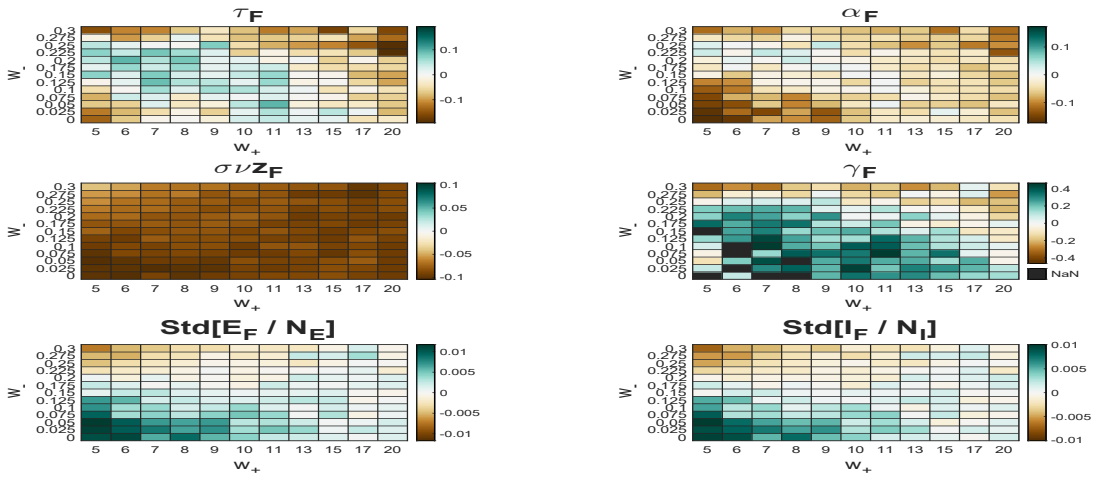

Figure 7: Differences between simulations and experiments of the avalanche power law exponents and the standard deviation of the E and I summed normalized activities for different parameters w_+ and w_-, for $g = 1Hz$, $q = 0.1Hz$, $h = 0.001, \lambda = 80\mu m$ Color encodes the simulation value minus the experimental value (i.e white signals are a perfect match)

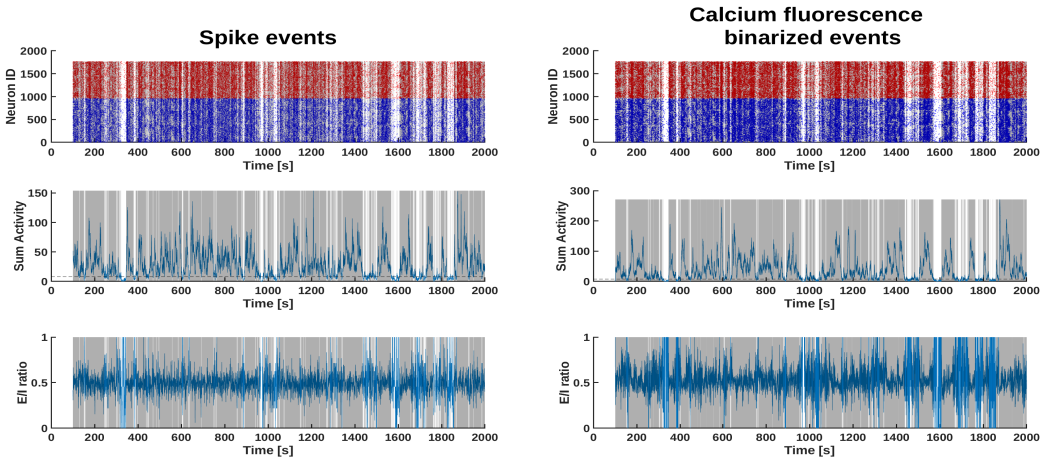

Figure 8: Example rasters, sum activity and E/I ratio with parameters $w_+ = 10$, $w_- = 0.1$, $g = 1Hz$, $q = 0.1Hz$, $h = 0.001, \lambda = 80\mu m$ producing calcium avalanches with exponents close to experimental data. Shaded patches show the occurring avalanches. E and I neurons in blue and red, respectively.

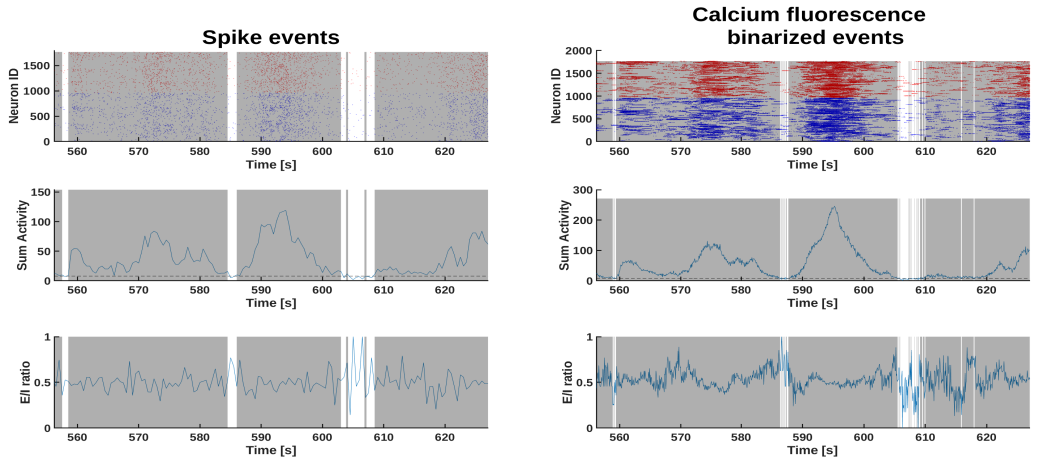

Figure 9: Zoom of Fig. 8 showing the effect of the convolution with the slow decaying double exponential kernel when converting from spikes to fluorescence (2.3)

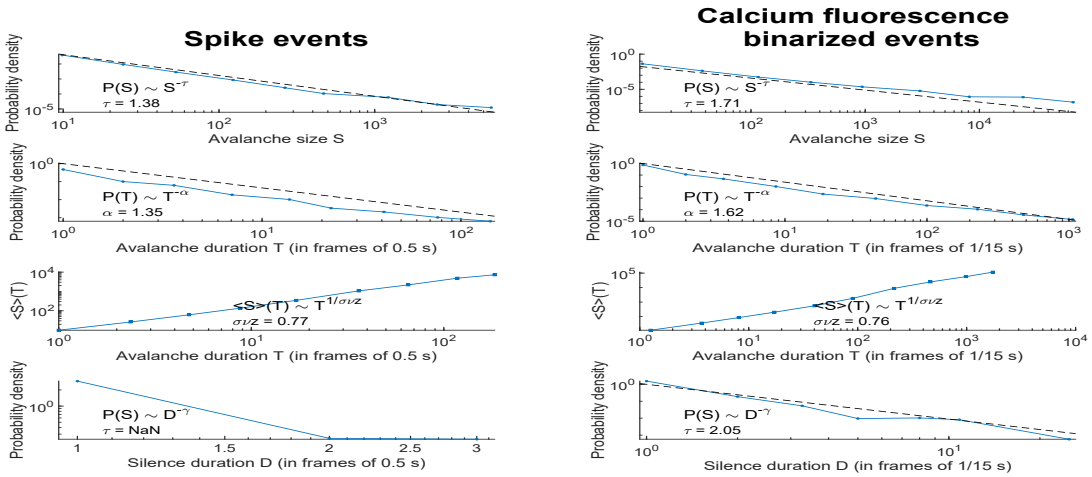

Figure 10: Avalanche distributions of Fig. 8 showing the resulting power law exponents (see Methods 2.5)

3.2 Simulations applying constant external stimuli, h_I and h_E, to E and I populations

Here we set the parameters $w_+ = 10, w_- = 0.09, \lambda = 80\mu m, h = 0.001$ found in the previous subsection 3.1 that generate calcium fluorescence binarized events with avalanche dynamics with avalanche power law statistics similar to those of the experimental data, and we explore the effect of varying the parameters of the external stimulus to the neurons $h_i(t)$ which could represent, e.g., optogenetic stimuli. First, in 3.2.1, we replace the uniform constant external stimulus $h = 0.001$, that all neurons receive, for h_E and h_I, applied to all E and I neurons, respectively. Then, in 3.2.2 and 3.2.3, we consider the uniform $h = 0.001$ constant background external stimulation identical for all neurons, and we add a second external stimulus, noted h_E or h_I again, applied to a certain proportion of E and I neurons, n_E and n_I. When presenting average values of statistics, the averages are meant to be over three simulations (see 2.6) of same duration $T_{max} = 2000$s.

3.2.1 Applying external stimuli to all E and I neurons

We varied the intensity of a constant external stimulus h_E and h_I, applied to the entire populations of E and I neurons ($n_E = n_I = 1$), respectively, for different combinations of (h_E,h_I). We start by distinguish among three types of qualitative behaviour by analyzing the spike rasters (Figs. 11,12). First, along the diagonal, $h_E = h_I$, avalanche dynamics are maintained up to the maximal value of stimulus $h_E = h_I = 0.05$ (Figs. 13, 14) and the spike and calcium power law exponents and the variances of the summed E and I activities remain almost constant (Fig. 19), as close to their experimental values as the parameters we found allows for (Fig. 20). Second, for $h_E = 0.05 > h_I \geq 0.0088$, we see big avalanches and short silences, coherent with the decrease in α, τ, the NaN values of γ and a slight decrease in variance of summed activity, as this summed activity gets closer to a sustained activity oscillating around a mean value without vanishing. And for even lower values of $h_I (\leq 0.0057)$, i.e. when h_E is unmatched, the dynamics is no longer avalanche-like but rather asynchronous Poissonian for both E and I neurons (e.g. Figs. 15, 16), with similar E and I firing rates and almost absence of total silence of the network.Third, for high values of $h_I (= 0.034)$ and low enough values of $h_E (\leq 0.0024)$, the I neurons visibly overinhibit the E neurons, and so avalanches are short and α, τ are big, and silences are big and γ is small (e.g. Figs. 17, 18), and when inhibition is even higher $h_I = 0.05, h_E \leq 0.0057$, the E neurons are totally inhibited while the I neurons remain active in a Poissonian regime driven by h_I. For parameters in between those three limit cases, one sees avalanche power laws (Fig. 21), with exponents varying following the same tendencies already described (Fig. 19). Notably, the power law exponents deviate from the experimental values when the mean E/I ratio deviates from the balance value of 0.5 (Fig. 22), analogously as the experimental exponents deviate from their critical value when the mean E/I ratio deviates from 0.5 (Fig. 3).

In summary, h_E tends to drive the network towards a regime of longer avalanches and shorter silences but keeping the E/I balance, until reaching a limit of nonstopping Poissonian E and I activity, whereas h_I tends to drive the network to shorter avalanches and longer silences while creating an E/I unbalance, until it makes the I neurons take completely over the E neurons, and, when combined, the effects of h_E and h_I compensate each other. Satisfactorily, the calcium statistics have a similar structure as the spike statistics. However, as the calcium signal is the result of the convolution of the spike with a slow decaying double exponential kernel with some noise, it decreases the silence period, so, naturally, the structure of the heatmaps of silences (captured in γ_F) and of variances get deformed.

One can try to give a broad explanation for these results : If both h_E and h_I are low, the stimuli start driving E and I, and as E recruits more I, I stops E and itself, until the cycle starts again, and so on average the E/I ratio is close to 0.5. If $h_E, h_I > 0.05$ are both too high, we have found (not shown) that they drive E and I towards a Poissonian regime where both E and I fire close to the maximum firing rate imposed by the model parameters (which is $\frac{qg}{q+g}$, as any possible negative synaptic input becomes negligible with respect to the positive external input, which saturates the nonlinearity), and again, the average the E/I ratio remains balanced. If $h_E > h_I$, h_E activates a big proportion of E, and so E activates also a big proportion of I ($\frac{I}{N_I} \sim 0.1$), and I tends to stop E but h_E is high enough to keep driving E, and thus I, for a long time which gives the bigger avalanches, and again on average the E/I ratio is close to 0.5. If $h_E >> h_I$, the unbalanced drive h_E does not allow activity to vanish, which gives the Poissonian regime,

still with balanced E/I. It is only when $h_I > h_E$ that the E/I balance is broken as h_I drives I and I stops E and also tends to stop itself, making avalanches shorter, but h_I is high enough to keep I in a Poissonian regime, which increases silences as it becomes more unlikely that E starts a new avalanche.

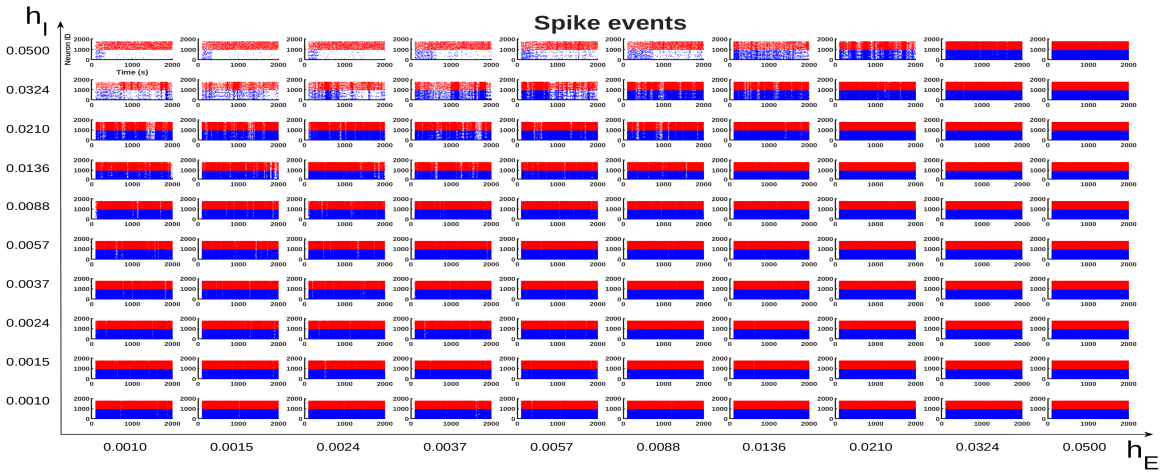

Figure 11: Spike rasters when varying over logarithmically spaced points between [0.001,0.05] the total inputs h_E and h_I to the entire E and I populations. Initial transient activity for $t < t_{eq} = 100$s is not taken into account

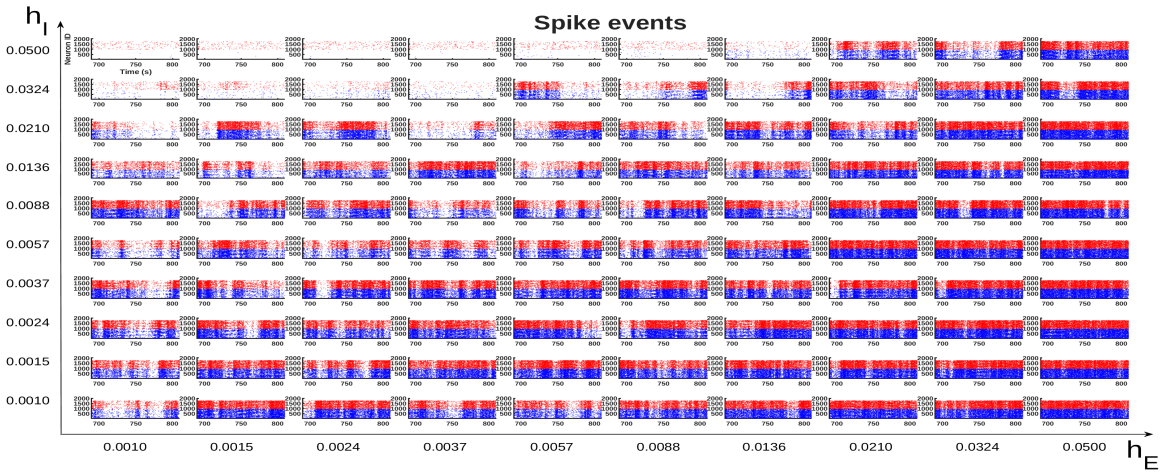

Figure 12: Zoom of Fig. 11

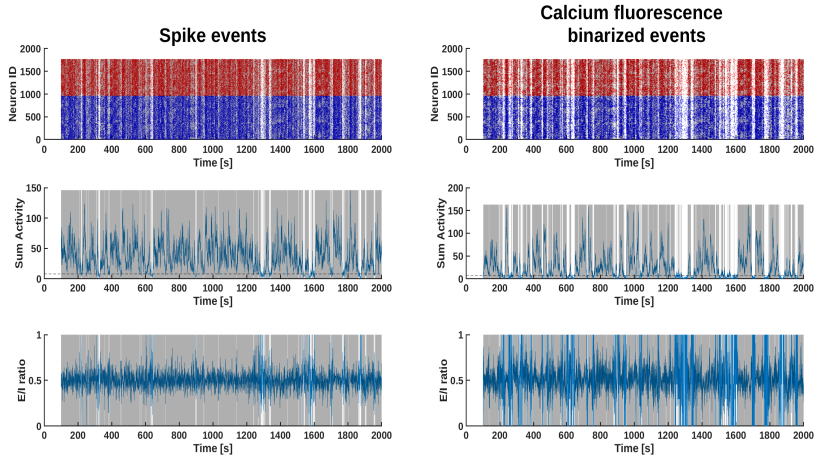

Figure 13: Sample rasters, sum activity and E/I ratio of a simulation for $h_E = h_I = 0.05$

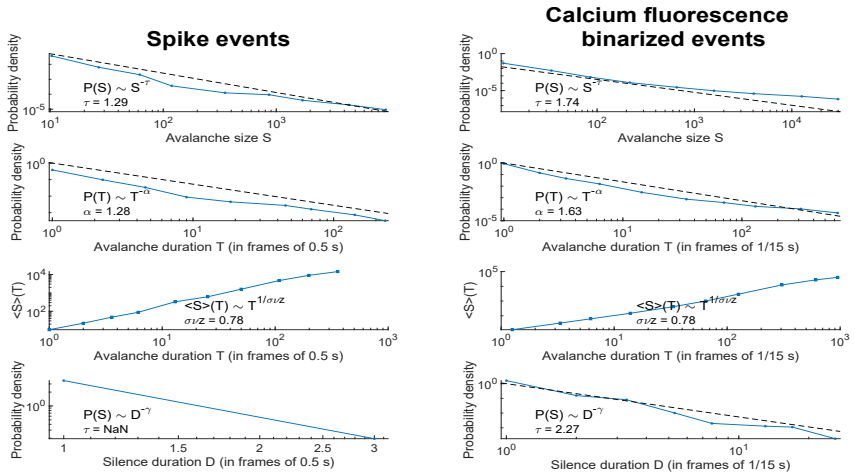

Figure 14: Avalanche distributions of Fig. 13 for $h_E = h_I = 0.05$

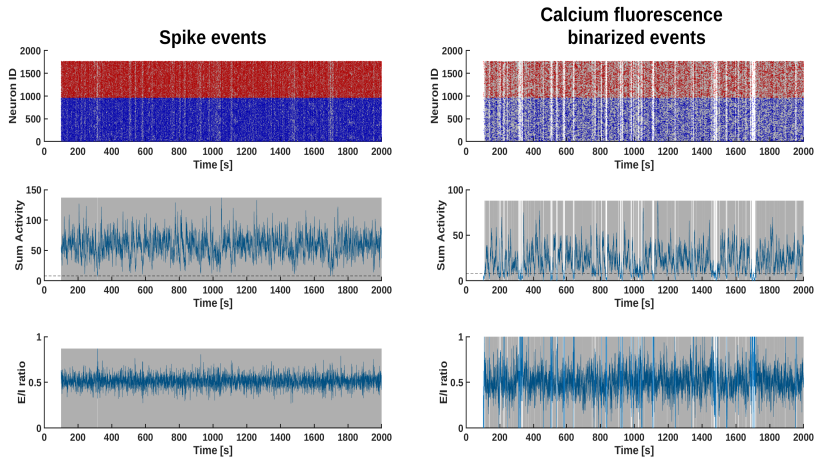

Figure 15: Sample rasters, sum activity and E/I ratio of a simulation for $h_E = 0.05 >> h_I = 0.001$

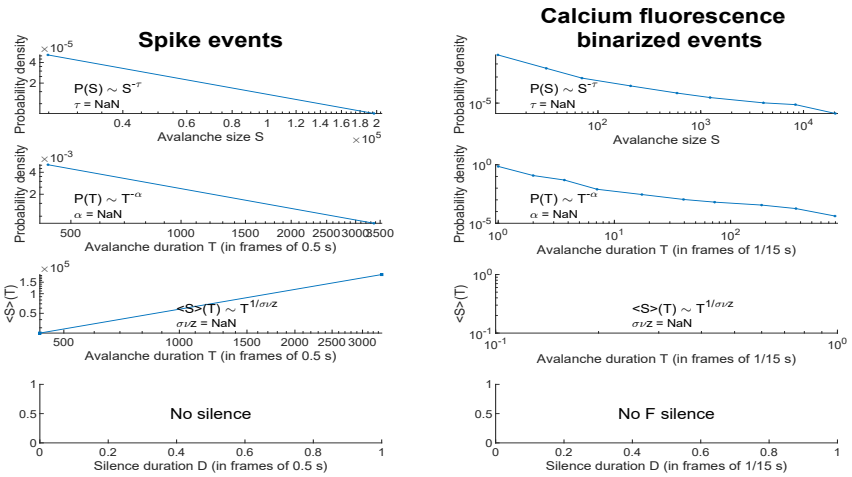

Figure 16: Avalanche distributions of Fig. 15 for $h_E = 0.05 >> h_I = 0.001$

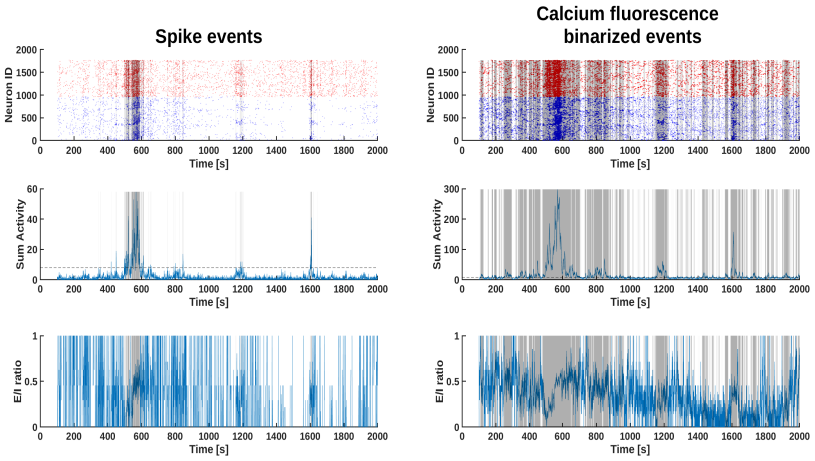

Figure 17: Sample rasters, sum activity and E/I ratio of a simulation for $h_I = 0.0324 >> h_E = 0.0024$

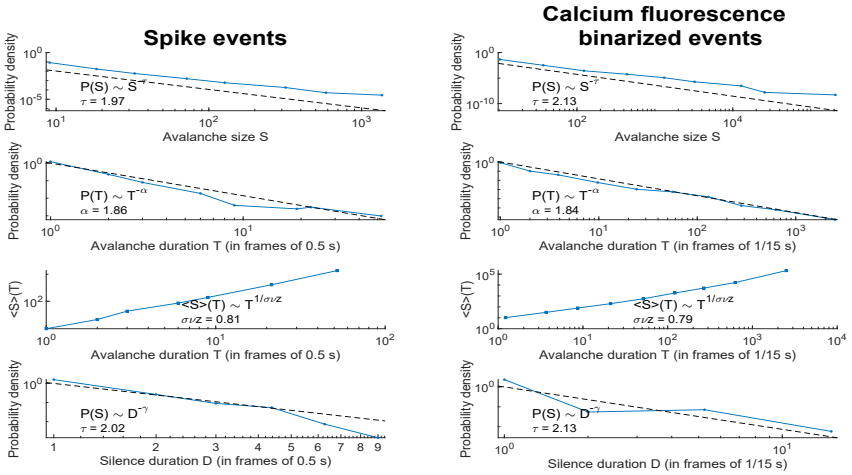

Figure 18: Avalanche distributions of Fig. 17 for $h_I = 0.0324 >> h_E = 0.0024$

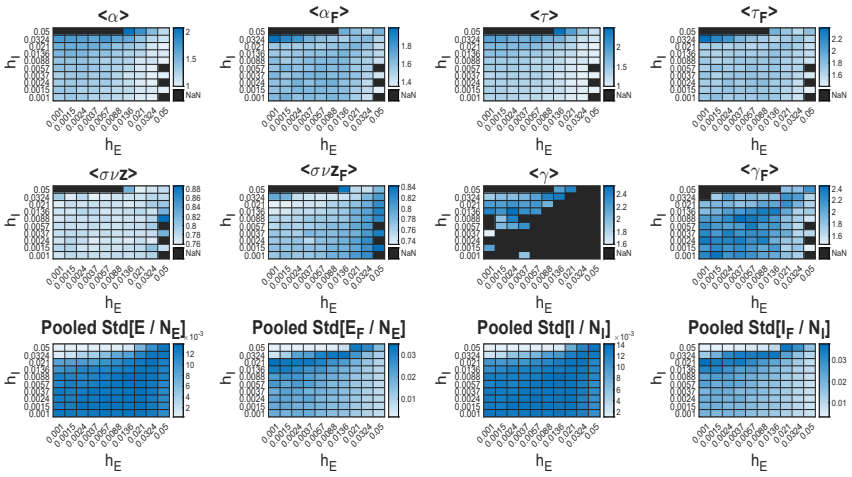

Figure 19: Average avalanche statistics over three simulations

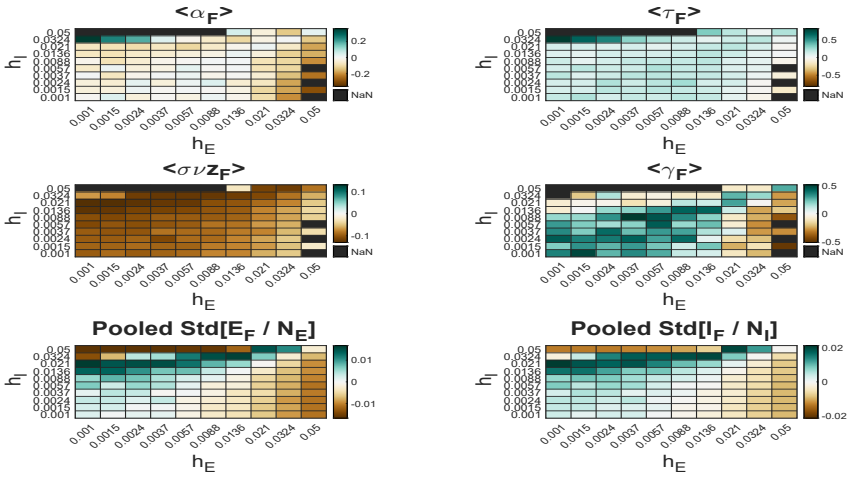

Figure 20: Difference between simulations and experimental avalanche statistics. Color encodes the simulation value minus the experimental value

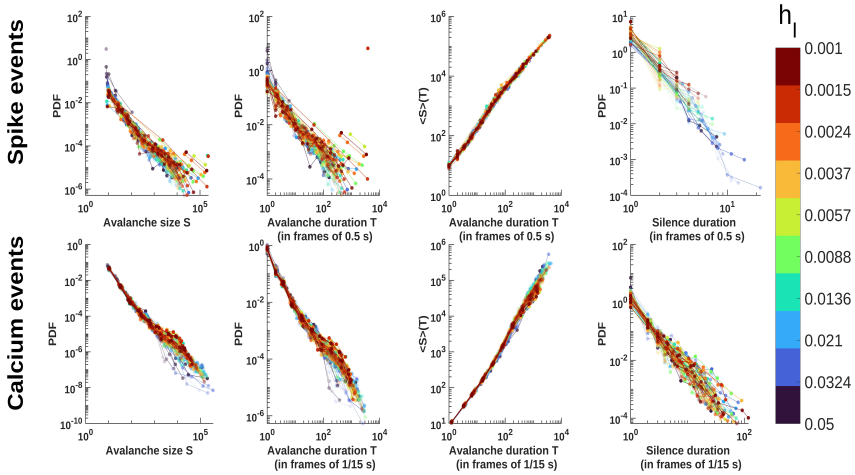

Figure 21: Avalanche distributions for one of the three simulation batches of those considered to produce the average exponents in Fig. 19. Less transparent colors mean higher values of h_E

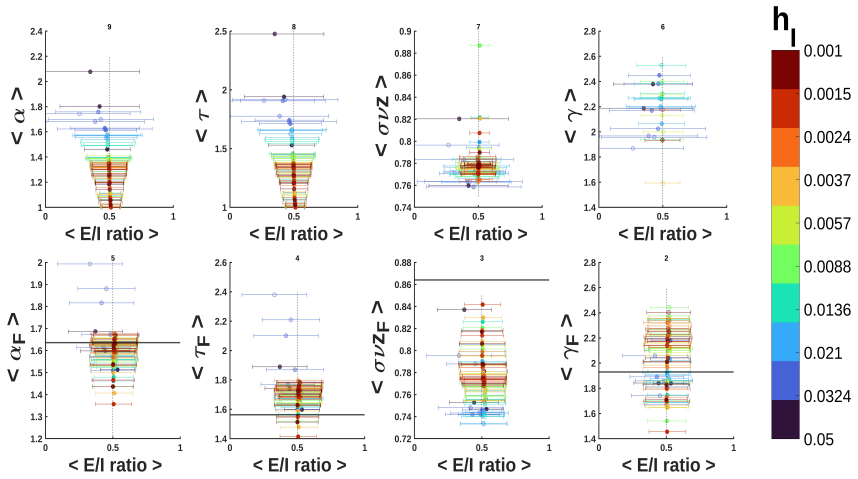

Figure 22: Relation between average over simulations of the power law exponents and average over simulations of the mean E/I ratio. Error bars are the pooled standard deviation (i.e., taking into account the standard deviations of the E/I ratio of each of the three simulations used for the average). Less transparent colors mean higher values of h_E

3.2.2 Appliying an external stimulus to a proportion of E neurons

We varied the intensity of a constant external stimulus h_E applied to a proportion n_E of E neurons, for different combinations of (h_E,n_E) (Fig. 24). Here, we observe the same role for h_E as discussed in 3.2.1, in which it drives the network towards longer avalanches and shorter silences, i.e smaller α, τ and makes γ take NaN values. The n_E parameter only modulates the effect of h_E (26,25,27). Again, the structure of the calcium and spike statistics heatmaps are similar, except for γ_F due to the noise introduced when transforming spikes to calcium events. Equally consistent with the explanations given in 3.2.1, we see that h_E can not increase the E/I ratio (it only deviates from 0.5 of ~ 0.02 for calcium when both h_E, n_E are high, see Fig. 23), as it can only turn the activity more Poissonian.

Interestingly, here we also see that this intuition on the role of h_E remains valid if one does a more "local" stimulation (e.g. $n_E = 0.2$) that, one could think, would not have enough nearby I to recruit, but rather would recruit nearby E and create a positive feedback loop that lasts long enough until more I is recruited, thus increasing the mean E/I ratio. This could be due to the fact that the connectivity matrix does not seem to have isolated islands of E or I neurons (Fig. 5b), so the inhibition can prevent quickly enough such loops in E occurring at any place in the network, and so the E/I ratio remains close to 0.5.

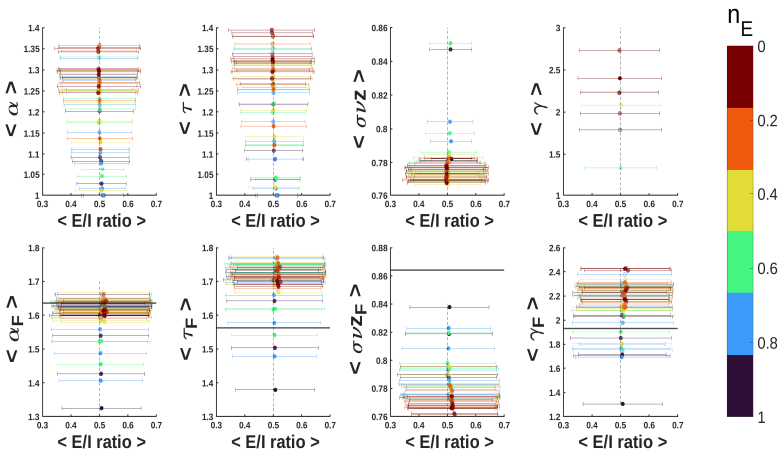

Figure 23: Relation between average over simulations of the power law exponents and average over simulations of the mean E/I ratio. Error bars are from the pooled standard deviation (i.e., taken into account the standard deviations of the E/I ratio of each of the three simulations used for taking the average). Less transparent colors mean higher values of h_E

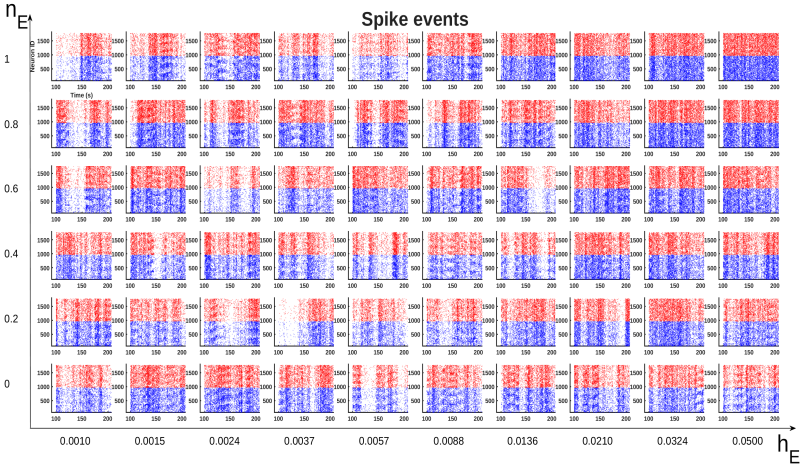

Figure 24: Spike rasters when varying over logarithmically spaced points between [0.001,0.05] the additional external input h_E and the proportion of neurons receiving this stimulus, n_E

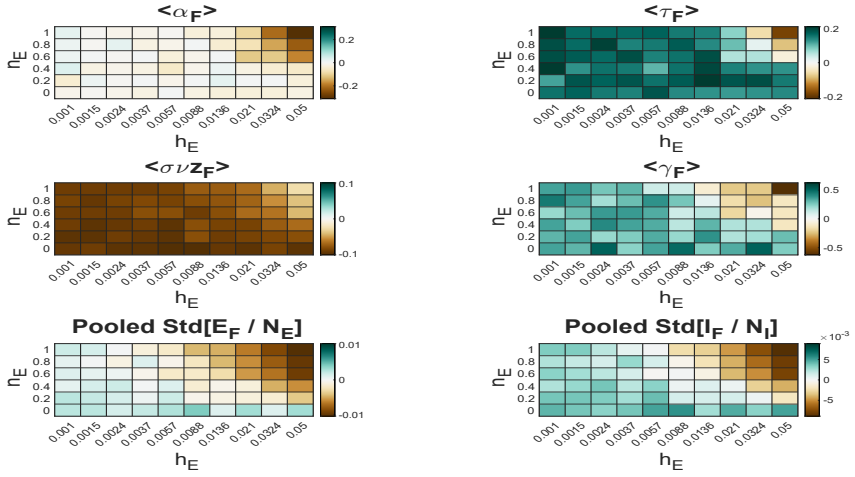

Figure 25: Difference between simulations and experimental avalanche statistics. Color encodes the simulation value minus the experimental value

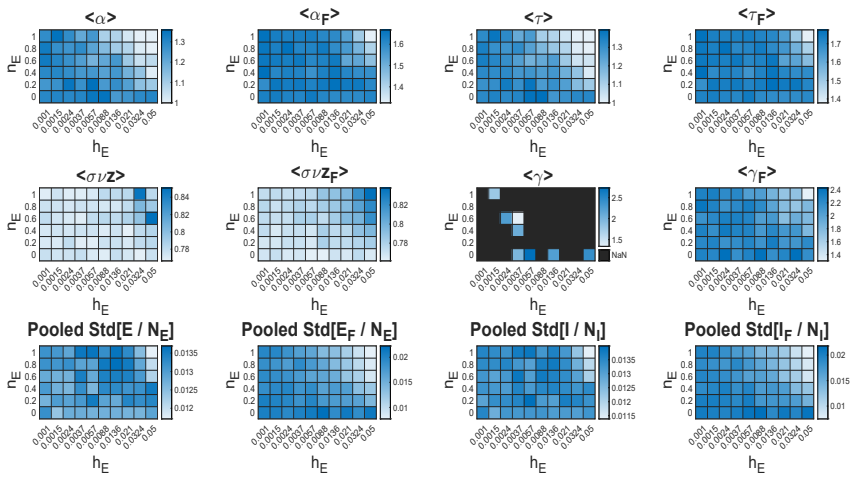

Figure 26: Average avalanche statistics over three simulations

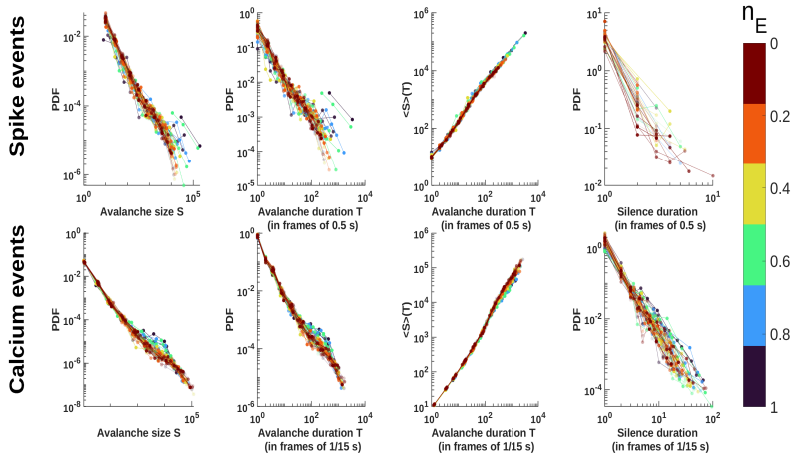

Figure 27: Avalanche distributions for one of the three simulation batches of those considered to produce the average exponents in 26. Less transparent colors mean higher values of h_E

3.2.3 Applying an external stimulus to a proportion of I neurons

We varied the intensity of a constant external stimulus h_I applied to a proportion n_I of I neurons, for different combinations of (h_I,n_I). Similarly to 3.2.2, the proportion of stimulated neurons, here n_I, only modulated the effects of h_I already discussed in 3.2.1. Note in Fig. 33 that for low n_I or low h_I the mode of the mean E/I ratio is ≈ 0.52 for calcium events, as it was the case when varying h_E and n_E in 3.2.2. Thus, this increase in E/I ratio should be interpreted as a deviation from balance, but as an artifact of the transformation from spikes to calcium (Figs. 30,31,32,28,29).

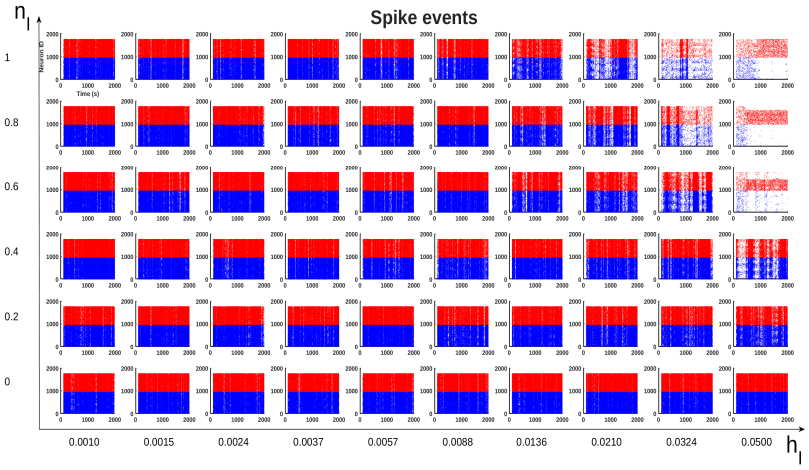

Figure 28: Spike rasters when varying over logarithmically spaced points between [0.001,0.05] the additional external input h_I and the proportion of neurons receiving this stimulus, n_I

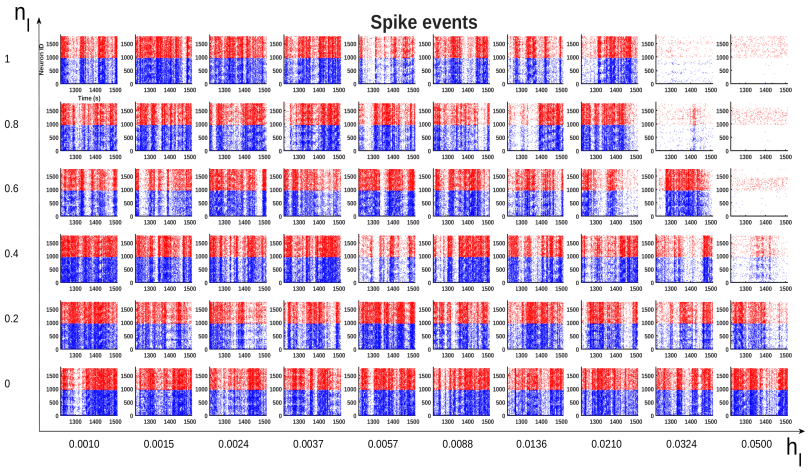

Figure 29: Zoom of 28

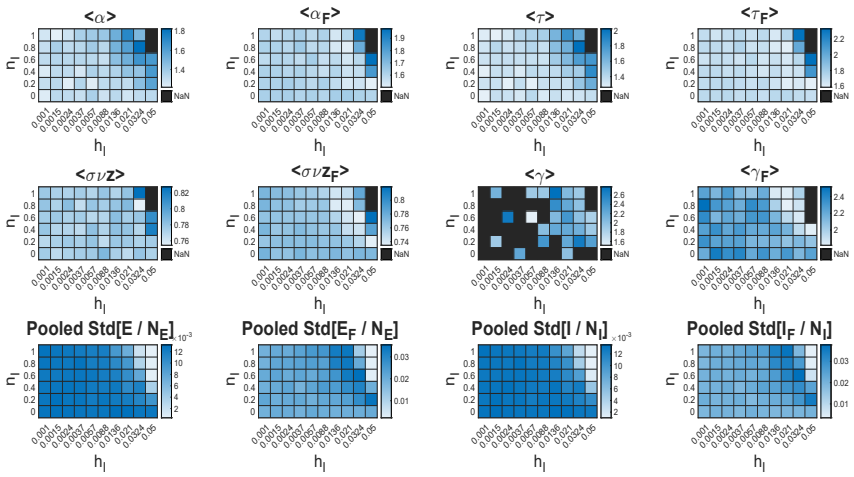

Figure 30: Average avalanche statistics over three simulations

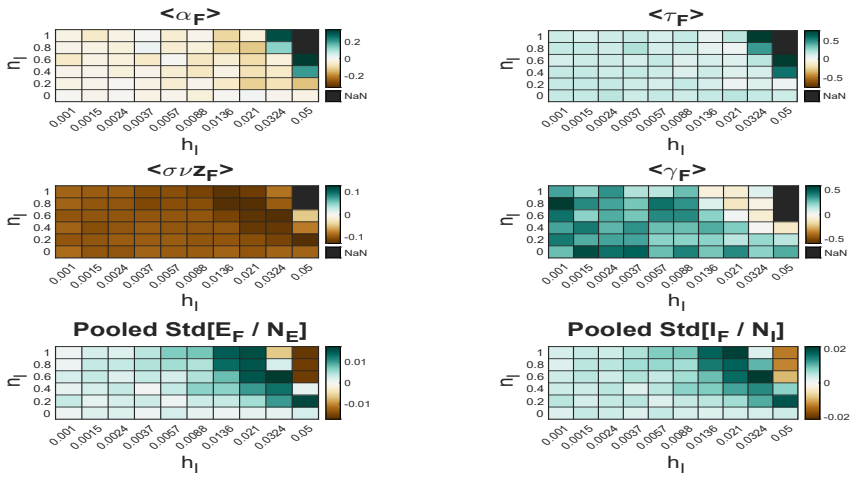

Figure 31: Difference between simulations and experimental avalanche statistics. Color encodes the simulation value minus the experimental value

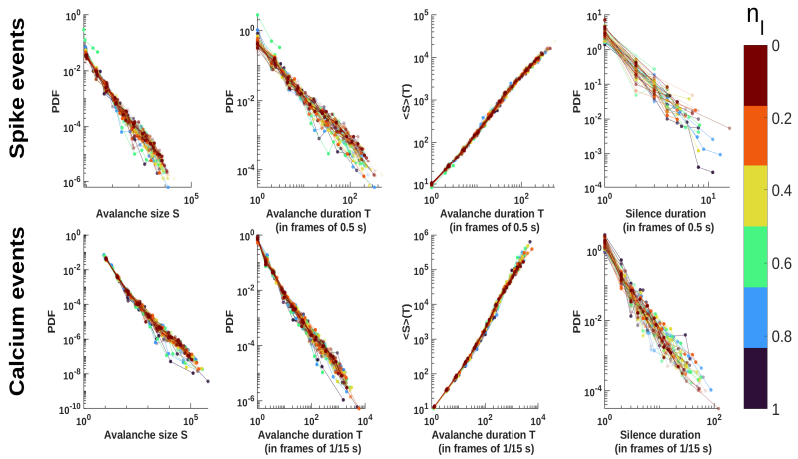

Figure 32: Avalanche distributions for one of the three simulation batches of those considered to produce the average exponents in 30.Less transparent colors mean higher values of h_I

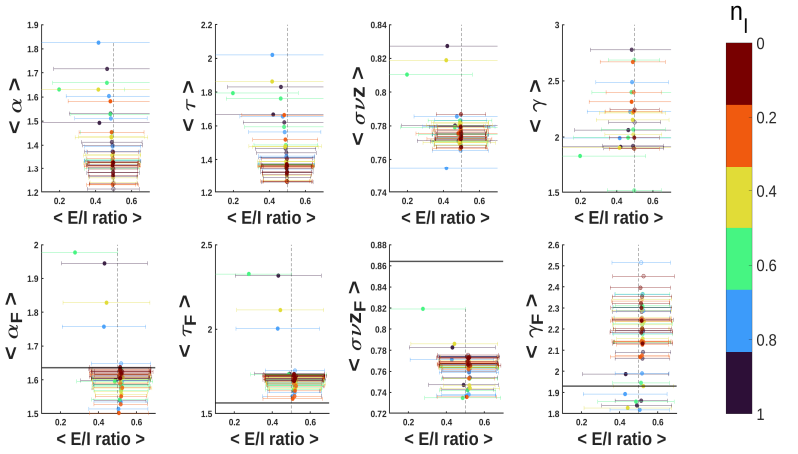

Figure 33: Relation between average over simulations power law exponents and average over simulations of mean E/I ratio. Error bars are from the pooled standard deviation (i.e., taken into account the standard deviations of the E/I ratio of each of the three simulations used for taking the average). Less transparent colors mean higher values of h_I

4 Conclusion

This work found parameters of the stochastic Wilson Cowan model that calcium event avalanches with power law statistics similar to those found in experimental data of the zebrafish optic tectum. When perturbing the spontaneous activity of both E and I populations with constant external stimuli of intensity h_E and h_I for the whole duration of the simulations, we found that there is an asymmetry between stimulating predominantly only one of the populations. When overly stimulating the E population, i.e., $h_E > h_I$, the avalanches get longer, and as h_E increases, the avalanche dynamics disappears and a Poissonian desynchronized regime establishes, but in any case the inhibition is capable of maintaining the E/I ratio close to its balance value of 0.5. However, when overly stimulating the I neurons, they make the avalanches shorter, the silences between avalanches longer and the E/I ratio lower, because, even though I neurons can inhibit themselves, they are receiving a constant drive. Therefore, trivially, when $h_I \gg h_E$, they suppress completely the E neurons, and they remain spiking in a Poissonian regime. Surprisingly, big balanced stimuli $h_E \approx h_I$ do not change the avalanche power law statistics, provided the stimuli do not get too big to saturate the non linear response function of the neurons, in which case the network goes to a Poissonian regime, firing close to the maximum firing rates imposed by the model. Finally, we have also seen that "local" stimulations to certain proportions of E or I neurons only modulate the effects of h_E and h_I already mentioned, but do not change their qualitative role, as the networks considered have a high degree of connectivity, making positive feedback loop between islands of E neurons rare.

Interesting continuations could include a study of the transient regimes when applying time dependent external stimuli to better understand how avalanches emerge and end (perhaps with analysis in the Fourier space), or to see if it is possible to phase lock the network. Other possibilities are the study of more realistic spatial profiles of stimulations (e.g., those of a laser doing an optogenetic stimulation), the influence of the change in spatial distribution of the neurons that is used to generate the connectivity matrix, e.g., to see if there are hub neurons or clusters (see 5.1) and a study of the relevance of initial conditions of the network. Additionally, to increase the E/I ratio, one could try to increase/decrease the number of excitatory/inhibitory neurons, which could represent and experiment where they are inactivated (e.g. with neuromodulation), which could give rise to E islands.

This work could also be further complemented by studying the effects of the threshold and bin sizes used when finding avalanches, and by studying the effects of the parameters of the kernel converting spikes to calcium events, as short calcium avalanches tend to get merged into bigger avalanches, which lowers the exponents and could possibly be contributing to some of the bumps in the power law distributions.

5 Supplementary Information

5.1 Variability across fishes

The parameters found to produce avalanche dynamics using the connectivity matrix as a function of the position of the neurons of one particular fish (see 3.1) did not generate avalanche dynamics for all fish (Figs. 35,34). Even though the number of neurons slightly increases in certain fish, which, as already described in 2.1, makes the deterministic, non-

avalanche dynamics, dominate over the fluctuations that produce the avalanche, this was found in Benayoun et al. [2010] to have effect for $N > 10^5$, whereas here in any case we stay in $N \sim 10^3$. Perhaps the difference lies in the spatial distribution of neurons that changes the connectivity matrix (see Fig. 36, where the spatial separation between E and I populations is more prominent than in Fig.5a).

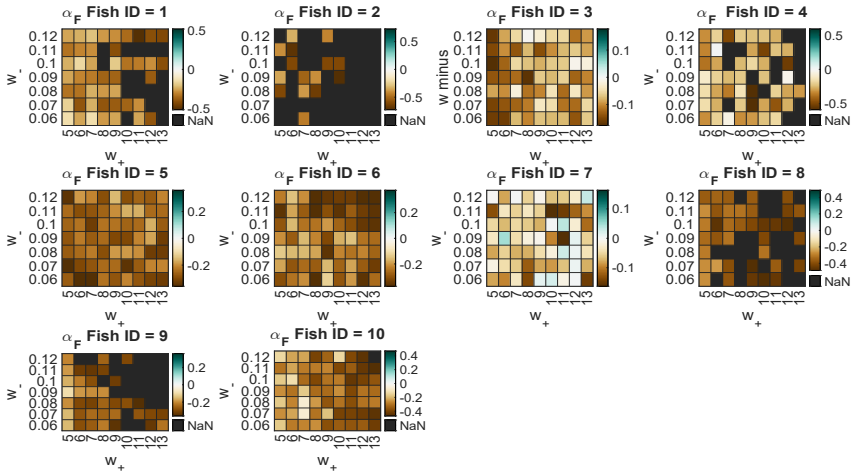

Figure 34: Results of the calcium events avalanche duration power law exponent when varying w_+, w_- for different fishes. Color encodes the simulation value minus the experimental value

Figure 35: Raster of fish ID = 8 with parameters that generate avalanches in fish ID = 3

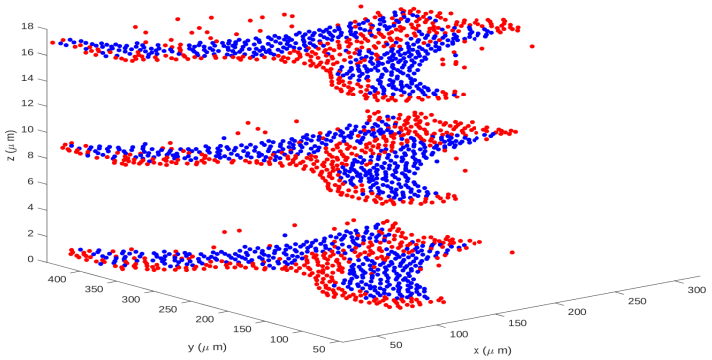

Figure 36: Positions of neurons for the fish ID = 8

5.2 Mean firing rates and q, g

Note that the parameters $q = 0.1Hz$, $g = 1Hz$ used in the simulations impose a maximum mean firing rate for a neuron of $\frac{qg}{q+g} \approx 1$Hz (think about the case of saturated inputs, where a neuron has then constant transition rates q and g), and commonly the firing rates are much lower than that ($\approx 0.01Hz$, not shown), which could be considered unrealistic, even for resting state neurons. However, this choice had to be made, as the conversion from spikes to calcium via a convolution with a slowly decaying double exponential kernel and the subsequent binarization is analogous to applying a low pass filter, which means that for higher firing rates, the signal is lost. We tried scaling up q, g to the expense of scaling down inputs, i.e, scaling down h, w_+, w_- to decrease the firing rates, however, as shown by analytic discussions of the SWC (de Candia et al. [2021b]), avalanches are produced for $w_- \sim \frac{g}{g}$ (Fig 37), and thus for more realistic values $q = 100Hz, g = 1000Hz$, the ratio $\frac{q}{g} = 0.1$ remains constant which constrains w_- not to be scaled down.

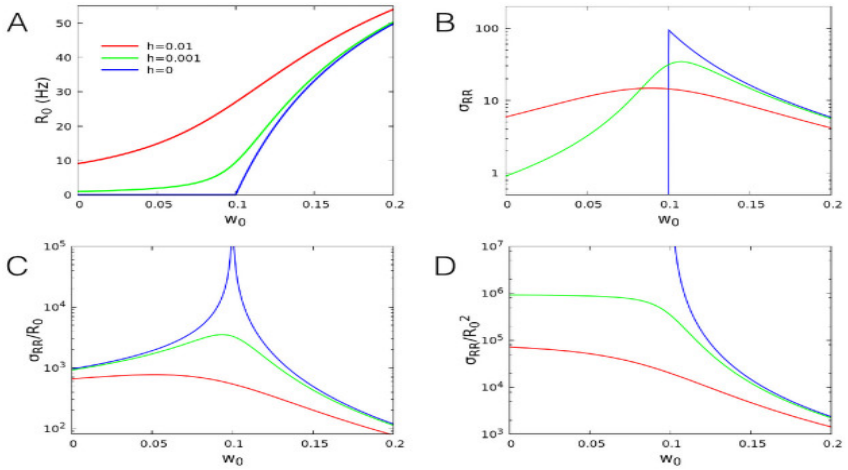

Figure 37: Figure and caption from de Candia et al. [2021a] : (A) Analytical dependence of the firing rate per neuron at the fixed point on the value of w_0, for different values of h. (B) Normalized variance $\sigma_{RR} = N < (R - R_0)^2 >$ as a function of w_0. (C) Fano factor σ_{RR}/R_0. (D) Square coefficient of variation σ_{RR}/R_0^2, that is equal to N times the variance of the ratio $\frac{R}{R_0}$. Other parameters: $\alpha = 0.1ms^{-1}, \beta = 1ms^{-1}, w_E + w_I = 13.8$

References

John M. Beggs and Dietmar Plenz. Neuronal avalanches in neocortical circuits. *The Journal of Neuroscience*, 23(35):11167–11177, December 2003. ISSN 1529-2401. doi: 10.1523/jneurosci.23-35-11167.2003. URL `http://dx.doi.org/10.1523/JNEUROSCI.23-35-11167.2003`.

Marc Benayoun, Jack D. Cowan, Wim van Drongelen, and Edward Wallace. Avalanches in a stochastic model of spiking neurons. *PLoS Computational Biology*, 6(7):e1000846, July 2010. ISSN 1553-7358. doi: 10.1371/journal.pcbi.1000846. URL `http://dx.doi.org/10.1371/journal.pcbi.1000846`.

Antonio de Candia, Alessandro Sarracino, Ilenia Apicella, and Lucilla de Arcangelis. Critical behaviour of the stochastic Wilson-Cowan model. *PLoS Comput. Biol.*, 17(8): e1008884, August 2021a.

Antonio de Candia, Alessandro Sarracino, Ilenia Apicella, and Lucilla de Arcangelis. Critical behaviour of the stochastic Wilson-Cowan model. *PLoS Comput. Biol.*, 17(8): e1008884, August 2021b. ISSN 1553-7358. doi: 10.1371/journal.pcbi.1008884.

Alain Destexhe and Jonathan D. Touboul. Is There Sufficient Evidence for Criticality in Cortical Systems? *eNeuro*, 8(2):0551–202021, April 2021. ISSN 2373-2822. doi: 10.1523/ENEURO.0551-20.2021.

Auriane Duchemin, Martin Privat, and Germán Sumbre. Fourier motion processing in the optic tectum and pretectum of the zebrafish larva. *Front. Neural Circuits*, 15: 814128, 2021.

Antonio J. Fontenele, Nivaldo A. P. de Vasconcelos, Thaís Feliciano, Leandro A. A. Aguiar, Carina Soares-Cunha, Bárbara Coimbra, Leonardo Dalla Porta, Sidarta Ribeiro, Ana João Rodrigues, Nuno Sousa, Pedro V. Carelli, and Mauro Copelli. Criticality between Cortical States. *Phys. Rev. Lett.*, 122(20):208101, May 2019. ISSN 1079-7114. doi: 10.1103/PhysRevLett.122.208101.

Antonio J. Fontenele, J. Samuel Sooter, V. Kindler Norman, Shree Hari Gautam, and Woodrow L. Shew. Low-dimensional criticality embedded in high-dimensional awake brain dynamics. *Science Advances*, 10(17), April 2024. ISSN 2375-2548. doi: 10.1126/sciadv.adj9303. URL `http://dx.doi.org/10.1126/sciadv.adj9303`.

Leandro J. Fosque, Rashid V. Williams-García, John M. Beggs, and Gerardo Ortiz. Evidence for Quasicritical Brain Dynamics. *Phys. Rev. Lett.*, 126(9):098101, March 2021. ISSN 1079-7114. doi: 10.1103/PhysRevLett.126.098101.

Nir Friedman, Shinya Ito, Braden A W Brinkman, Masanori Shimono, R E Lee DeVille, Karin A Dahmen, John M Beggs, and Thomas C Butler. Universal critical dynamics in high resolution neuronal avalanche data. *Phys. Rev. Lett.*, 108(20):208102, May 2012.

Daniel T. Gillespie. Exact stochastic simulation of coupled chemical reactions. *The Journal of Physical Chemistry*, 81(25):2340–2361, December 1977. ISSN 1541-5740. doi: 10.1021/j100540a008. URL `http://dx.doi.org/10.1021/j100540a008`.

Gerald Hahn, Thomas Petermann, Martha N. Havenith, Shan Yu, Wolf Singer, Dietmar Plenz, and Danko Nikolić. Neuronal Avalanches in Spontaneous Activity In Vivo. *J. Neurophysiol.*, 104(6):3312, December 2010. doi: 10.1152/jn.00953.2009.

Takashi Kawashima, Maarten F Zwart, Chao-Tsung Yang, Brett D Mensh, and Misha B Ahrens. The serotonergic system tracks the outcomes of actions to mediate short-term motor learning. *Cell*, 167(4):933–946.e20, November 2016.

Najja Marshall, Nicholas M Timme, Nicholas Bennett, Monica Ripp, Edward Lautzenhiser, and John M Beggs. Analysis of power laws, shape collapses, and neural complexity: New techniques and MATLAB support via the NCC toolbox. *Front. Physiol.*, 7:250, June 2016.

Thomas Petermann, Tara C. Thiagarajan, Mikhail A. Lebedev, Miguel A. L. Nicolelis, Dante R. Chialvo, and Dietmar Plenz. Spontaneous cortical activity in awake monkeys composed of neuronal avalanches. *Proc. Natl. Acad. Sci. U.S.A.*, 106(37):15921–15926, September 2009. doi: 10.1073/pnas.0904089106.

Dietmar Plenz, Tiago L. Ribeiro, Stephanie R. Miller, Patrick A. Kells, Ali Vakili, and Elliott L. Capek. Self-Organized Criticality in the Brain. *Front. Phys.*, 9:639389, July 2021. ISSN 2296-424X. doi: 10.3389/fphy.2021.639389.

Simon-Shlomo Poil, Richard Hardstone, Huibert D Mansvelder, and Klaus Linkenkaer-Hansen. Critical-state dynamics of avalanches and oscillations jointly emerge from balanced excitation/inhibition in neuronal networks. *J. Neurosci.*, 32(29):9817–9823, July 2012.

Adrián Ponce-Alvarez, Adrien Jouary, Martin Privat, Gustavo Deco, and Germán Sumbre. Whole-brain neuronal activity displays crackling noise dynamics. *Neuron*, 100 (6):1446–1459.e6, December 2018. ISSN 0896-6273. doi: 10.1016/j.neuron.2018.10.045. URL `http://dx.doi.org/10.1016/j.neuron.2018.10.045`.

Sebastián A Romano, Verónica Pérez-Schuster, Adrien Jouary, Jonathan Boulanger-Weill, Alessia Candeo, Thomas Pietri, and Germán Sumbre. An integrated calcium imaging processing toolbox for the analysis of neuronal population dynamics. *PLoS Comput. Biol.*, 13(6):e1005526, June 2017.

Or A. Shemesh, Changyang Linghu, Kiryl D. Piatkevich, Daniel Goodwin, Orhan Tunc Celiker, Howard J. Gritton, Michael F. Romano, Ruixuan Gao, Chih-Chieh (Jay) Yu, Hua-An Tseng, Seth Bensussen, Sujatha Narayan, Chao-Tsung Yang, Limor Freifeld, Cody A. Siciliano, Ishan Gupta, Joyce Wang, Nikita Pak, Young-Gyu Yoon, Jeremy F.P. Ullmann, Burcu Guner-Ataman, Habiba Noamany, Zoe R. Sheinkopf, Won Min Park, Shoh Asano, Amy E. Keating, James S. Trimmer, Jacob Reimer, Andreas S. Tolias, Mark F. Bear, Kay M. Tye, Xue Han, Misha B. Ahrens, and Edward S. Boyden. Precision calcium imaging of dense neural populations via a cell-body-targeted calcium indicator. *Neuron*, 107(3):470–486.e11, August 2020. ISSN 0896-6273. doi: 10.1016/j.neuron.2020.05.029. URL `http://dx.doi.org/10.1016/j.neuron.2020.05.029`.

Woodrow L. Shew and Dietmar Plenz. The functional benefits of criticality in the cortex. *Neuroscientist*, 19(1):88–100, February 2013. ISSN 1089-4098. doi: 10.1177/1073858412445487.

Ziqiang Wei, Bei-Jung Lin, Tsai-Wen Chen, Kayvon Daie, Karel Svoboda, and Shaul Druckmann. A comparison of neuronal population dynamics measured with calcium imaging and electrophysiology. *PLOS Computational Biology*, 16(9):e1008198, September 2020. ISSN 1553-7358. doi: 10.1371/journal.pcbi.1008198. URL `http://dx.doi.org/10.1371/journal.pcbi.1008198`.

H. R. Wilson and J. D. Cowan. Excitatory and inhibitory interactions in localized populations of model neurons. *Biophys. J.*, 12(1):1–24, January 1972. ISSN 0006-3495. doi: 10.1016/S0006-3495(72)86068-5.